Journal of Materials Research and Technology 29 (2024) 1010–1024

Contents lists available at ScienceDirect

Journal of Materials Research and Technology

journal homepage: www.elsevier.com/locate/jmrt

Evaluating the versatility of stainless steel flakes and magnetite powder as polyvalent additives for wood paints

Massimo Calovi *, Stefano Rossi

Department of Industrial Engineering, University of Trento, Via Sommarive 9, 38123, Trento, Italy

ARTICLE INFO

Handling editor: M Meyers

Keywords:
Stainless steel flakes
Magnetite powder
Wood paint
Protective coating
Electrical conductivity
Magnetic paint

ABSTRACT

The objective of this study is to evaluate how various fillers, specifically stainless steel flakes and magnetite powder, affect the visual attributes, durability and versatility of a water-based wood paint. To examine the influence of these two specific pigments on the overall look of the coatings, colorimetric measurements were carried out. The impact of these distinct fillers on the durability of the layers was assessed by subjecting the samples to xenon arc light exposure and cyclic thermal shocks, followed by colorimetric inspections and adhesion tests. Furthermore, the fillers' impact on the coating's ability to act as a barrier was assessed through liquid resistance and water uptake tests. Additionally, the Buchholz hardness indentation test and the Taber test were conducted to quantify how these functional additives affect the mechanical properties of the coatings, such as hardness and resistance to abrasion. Lastly, two specific tests revealed the fillers' role in introducing unique electrical conductivity and magnetic attractive properties to the paint. In conclusion, this study underscores the intriguing influence of stainless steel flakes and magnetite powder, which not only impart vibrant colors and distinct visual characteristics to the paint but also maintain the coating's protective barrier properties, enhance the mechanical properties of the composite layer, and introduce specific multifunctional features to the coating.

1. Introduction

The coatings sector has always played a pivotal role in the economies of many countries [1], as the preservation of components and their durability has a significant economic impact [2]. For this reason, over the years, coatings have been the subject of various innovative studies aimed at further enhancing the protective properties of layers to extend the service life of industrial components [3]. Today, it is taken for granted to expect a coating to exert a significant protective influence on the substrate to which it is applied. Moreover, current trends also involve substantial aesthetic considerations, including color, gloss, and texture of the protective layer. So, the coating cannot only serve a protective function but also be aesthetically pleasing [4].

However, a current and rapidly growing trend believes that a single coating should not only be protective and visually appealing but also capable of offering additional functionalities [4]. For instance, it should possess good abrasion resistance [5], be responsive to external stimuli such as temperature [6] or light [7], express bactericidal activity [8] and incorporate additives that can introduce thermal and electrical conductivity features [9,10], which can be appreciated in highly technological industrial fields. These aspects pertain to metallic [11] and ceramic coatings [12] but are also predominantly associated with organic coatings [13].

Paints are one of the most widely used coatings globally, applied on both metallic and wooden substrates. Specifically, wood has always been one of the most utilized materials [14] in various industrial sectors, valued for its ease of workability [15], specific chemical [16] and physical [17] attributes and natural abundance. Moreover, during a time in history when significant emphasis is placed on environmental conservation, wood is also viewed favorably as a renewable and biodegradable material that has no CO_2 footprint.

However, wood requires proper precautions, such as the application of protective coatings [18,19], in order to reduce the physical-chemical degradation of its lignocellulosic components caused by solar radiation [20], moisture penetration into its structure [21], limit potential mechanical damage [22] or damage caused by chemicals [23], or safeguard the wood from harmful microorganisms such as fungi [24,25]. In this context, wood coatings have been the subject of various studies aimed at improving their protective properties, often through the incorporation of specific functional fillers [26]. For example, metallic and ceramic

* Corresponding author.
E-mail address: massimo.calovi@unitn.it (M. Calovi).

https://doi.org/10.1016/j.jmrt.2024.01.171
Received 30 November 2023; Received in revised form 8 January 2024; Accepted 18 January 2024
Available online 22 January 2024
2238-7854/© 2024 The Author(s). Published by Elsevier B.V. This is an open access article under the CC BY license (http://creativecommons.org/licenses/by/4.0/).

nanopowders have demonstrated an effective shielding effect against UV radiation [27–29] or played a key role in increasing the hardness and stiffness of the wood [30–32], as well as significantly reducing water uptake phenomena in the coating [33]. Finally, metallic nanomaterials have been used to impart effective antibacterial and fungicidal functions to the coating [34–36].

Nevertheless, the contemporary wood coatings sector is focusing on specific visual attributes to achieve vivid layers of color [37] by exploring and creating novel pigments [38]. In this regard, recent research [39,40] has delved into the durability of these pigment sources in wooden coatings. Yet, a significant hurdle when employing these new pigments is striking a balance between their dual roles of aesthetics and protection. They must deliver unique visual effects while maintaining the protective barrier qualities of the organic coating. Considering, obviously, the multifunctionality aspects mentioned previously.

From this standpoint, stainless steel flakes and magnetite powder present appealing options for incorporating fresh visual elements and multifaceted characteristics into wood coatings. Indeed, these two substances, besides possessing distinct colors, also exhibit intriguing magnetic properties that have not been previously associated with wood paints. For instance, stainless steel flakes have been employed in recent studies to enhance the mechanical characteristics of organic matrix composites [41] and to elevate the resistance to abrasion in both organic [42,43] and inorganic coatings [44,45]. Moreover, the stainless steel flakes are part of the High-Performance Pigments family [46], metallic effect pigments [47,48] highly regarded by the current pigment industry. Likewise, magnetite micropowders were introduced into organic coatings to assess their influence on the layer's corrosion resistance [49], enhance adhesion and flame retardant properties of the film [50], and introduce self-repairing capabilities [51].

However, even with these considerations, neither stainless steel flakes nor magnetite powder have ever been used in wood coatings. Hence, this study seeks to explore the versatile influence of two distinct additives, namely stainless steel flakes and magnetite powder, on the performance of a water-based wood paint. The research not only assesses the aesthetic and multifunctional attributes introduced by these additives but also scrutinizes how the they affect the durability of the polymer coating when subjected to accelerated degradation tests. Lastly, the research delves into the multifunctional role of each filler separately, investigating their impact on the mechanical, electrical, and magnetic properties of the composite coating.

To enable a direct comparison of their performance, an equal quantity of fillers was individually incorporated into a commercial water-based paint. The influence of these fillers on the composite layers' structure and aesthetic properties was evaluated through a combination of scanning electron microscope (SEM) imaging, colorimetric assessment, and gloss analysis. This comprehensive approach was employed to characterize the impact of these additives on both the morphological characteristics and the appearance of the coatings. The influence of the fillers on the coatings' durability was assessed through two distinct accelerated degradation tests: exposure in a climatic chamber and in a xenon chamber. The primary objectives were to evaluate the barrier properties and the stability in terms of protection against color alteration. To monitor potential deterioration of the coatings, colorimetric analyses were conducted, tracking any associated aesthetic changes. Additionally, the cross-cut test was utilized to gauge the impact of thermal shocks on the adhesion of the coatings. Furthermore, the protective effectiveness of the coatings was examined through a chemical resistance test and a liquid water uptake test, with an analysis of potential color changes in the samples, to determine whether the fillers had any influence on the paint's barrier characteristics. Lastly, the multifunctional contribution of the two fillers was scrutinized with regards to abrasion resistance, electrical conductivity, and the magnetic properties exhibited by the paint.

2. Materials and methods

2.1. Materials

The Eckart Italia company (Rivazzano, PV, Italy), provided the lamellar stainless steel flakes labeled as STAY/STEEL LN 25, and these were used in their original state. The flakes have apparent density ranging from 0.2 to 0.4 g/cm^3 and are composed of stainless steel AISI 6126, with a composition of 10.0–20.0 wt% Cr – <0.1 wt% Ni – <1.0 wt % Co – 2.5–10.0 wt% Mn – 1.0–5.0 wt% Mo – Fe bal. The supplier's dimensional analysis specifies that the values for D10, D50, and D90 are in the ranges of 3.0–10.0, 20.0–27.0, and 35.0–55.0 μm, respectively. The magnetite powder was supplied by 2Dto3D, (Torino, Italy) and used as received. The material consists of a minimum of 95 % Fe_3O_4 and exhibits manufacturer-specified D50 and D90 values of 35 μm and 80 μm, respectively. The poplar wood panels, measuring 150 × 150 × 2 mm^3 in dimension, were sourced from Cimadom Legnami (Lavis, TN, Italy). The waterborne acrylic paint, denoted as TECH20, was procured from ICA Group (Civitanova Marche, AN, Italy). This paint formulation is derived from feedstocks originating from sustainable and renewable sources. Sodium chloride (with a minimum purity of 99.0 %) and ethanol (with a purity of 99.8 %) were acquired from Sigma-Aldrich (St. Louis, MO, USA), and were utilized in their original form. For liquid resistance assessments, the following products were procured: Suma Bac D10 Cleaner and Sanitiser, a commercial detergent disinfectant product by Diversey (Fort Mill, SC, USA), which contains benzalkonium chloride within the range of 3.0–10.0 wt%, and Catafor 502XC cataphoretic red ink manufactured by Arsonsisi (Milan, Italy).

2.2. Samples production

To attain a smooth texture, the initial step involved sanding the poplar wood panels with 320 grit paper. Consequently, the commercial paint formulation was adjusted by introducing stainless steel flakes and magnetite powder, respectively, to achieve a total filler content of 30 wt % in both the formulations. The choice of this amount was based on initial tests that demonstrated satisfactory multifunctional properties in both solutions. While the paint and coatings industry commonly operates using pigment volume concentration (PVC) [52,53], the two sets of fillers were added at identical weight percentages to emphasize the impact of their varying densities. This emphasis was crucial as it led to entirely distinct multifunctional performances, as elaborated in paragraph 3. Subsequently, the two paint blends underwent mechanical mixing for a duration of 30 min before application. Therefore, the paints were applied through spraying onto the prepared hardwood surfaces and allowed to air dry for a duration of 4 h at room temperature. This deposition and curing cycle was repeated twice. The application of the paint followed the supplier's recommendations, utilizing a pressure level of 3 bar and an application rate of 100 g/m^2. Consequently, the study assessed the impact of the two distinct fillers in the coatings, as outlined in Table 1, which presents the naming conventions for the three sample series considered in this research. The performances of the two samples containing the stainless steel flakes and the magnetite powder were compared with the behavior of sample REF, produced as a reference as it has no fillers added to the commercial paint.

Table 1
Sample naming convention.

Samples nomenclature	category of additivated filler (30 wt%)
REF	/
SSF	Stainless steel flakes
MAG	Magnetite powder

2.3. Characterization

The SEM analysis was conducted using the JEOL IT 300 low vacuum scanning electron microscope (JEOL, Akishima, Tokyo, Japan) to evaluate the characteristics of the two fillers and to examine the surface and cross-sectional morphology of the coatings. The objective was to assess how both the flakes and magnetite influenced the compactness and structural morphology of the layers.

The visual attributes of the coatings were assessed using colorimetric analysis conducted with a Konica Minolta CM-2600d spectrophotometer (Konica Minolta, Tokyo, Japan) in SCI mode, utilizing a D65/10° illuminant/observer configuration. Gloss measurements were performed using an Erichsen 503 instrument (Erichsen Cofomegra Instruments, Milan, Italy), following the ASTM D523/14 standard [54].

Two accelerated degradation tests were conducted to simulate exposure to severe conditions, with the aim of subjecting the coatings to particular stresses and evaluating potential changes in the durability of the layers resulting from the introduction of the flakes and the magnetite in the commercial paint.

In accordance with the ASTM G155-05 standard [55], the samples were placed in a Xenon Arc Light Apparatus Q-SUN Xe-1 Xenon Test Chamber (Q-Lab Corporation, Westlake, OH, USA) for a duration of 300 h (60 W/m^2 – 50 °C) to assess the resistance of the coatings to the degradation caused by exposure to solar radiation. The physical decay of the composite layers was evaluated by means of colorimetric analyses and gloss measurements.

To assess the impact of the two fillers on the paint's thermal resistance, the samples were subjected to drastic temperature variations using the ACS DM340 climatic chamber (Angelantoni Test Technologies, Perugia, Italy). The exposure test, as per the UNI 9429 standard [56], consisted of 15 cycles, each comprising.

- 4 h at +50 °C with relative humidity below 30 %;
- 4 h at −20 °C;
- 16 h at ambient temperature.

To prevent undesired moisture absorption by the poplar wood samples measuring 70 × 70 × 2 mm^3, silicone was employed to seal their five untreated surfaces. At intervals of every three exposure cycles in the climatic chamber, colorimetric investigations were performed to document any alterations in the coatings' appearance over the course of the test. Additionally, optical microscope Nikon SMZ25 (Nikon Instruments Europe, Amstelveen, the Netherlands) examinations were carried out to detect the possible development of micro-defects at the conclusion of the test. Likewise, the cross-cut test was executed following the ASTM D3359-17 standard [57] to assess potential variations in coating adhesion resulting from the alternating thermal cycles.

The impact of the two unique fillers on the acrylic matrix's ability to act as a barrier was investigated using chemical resistance tests in accordance with the GB/T 1733-93 standard [58]. Filter paper was immersed in four distinct solutions: 15 % sodium chloride, 70 % ethanol, detergent, and red ink. Subsequently, each saturated filter paper was positioned onto the coating surface and covered with a glass sheet. After a 24-h period, the glass cover and filter paper were removed, and any remaining liquid on the coating surface was absorbed. Colorimetric analyses were then employed to assess any imprints and changes in color. Additionally, the liquid water absorption test was conducted in accordance with the EN 927–5:2007 standard [59] to assess the water permeability of the coatings. The five uncoated surfaces of the 40 × 40 × 2 mm^3 poplar wood panels were hermetically sealed with silicone, using the same sealing procedure as employed during exposure in the climatic chamber, to prevent water absorption by the wood substrate. The samples were pre-conditioned at 65 % relative humidity and 20 °C, following which they were placed to float in a container filled with water. The moisture absorption, expressed in grams per square meter (g/m^2), was calculated by monitoring the change in mass before and after 6, 24, 48, 72, and 96 h.

The influence of the two fillers on the mechanical properties of the acrylic matrix was examined through both the Buchholz hardness indentation test and the Taber test. The Buchholz test, conducted in compliance with the ISO 2815 standard [60], involved measuring the length of the indentation created by the standardized instrument. Taber tests were conducted with a TABER 5135 Rotary Platform Abrasion Tester (Taber Industries, North Tonawanda, NY, USA) following the guidelines specified in the ASTM D4060-19 standard [61], employing two CS17 abrasion wheels. The samples underwent a total of 3000 Taber cycles, during which the extent of mass loss was monitored. Additionally, after completing the test, the abrasion profile was assessed using a roughness meter Waveline W600 (OGP HOMMEL, Desio, MB, Italy) to evaluate how the two fillers contributed to reducing abrasive wear. Lastly, the SEM was employed to observe the sample morphology, providing insights into how the two additives responded to the abrasive phenomenon.

Lastly, the multifunctional characteristics of the two filler types were evaluated, focusing on electrical conductivity and magnetic properties. The electrical conductivity of the coatings, influenced by both fillers, was assessed in accordance with the ASTM D257-07 standard [62], as previously detailed in earlier research [63,64]. This involved positioning two parallel silver paste electrodes (measuring 100 mm × 5 mm) on the sample's surface, separated by a 10 mm distance. The VersaSTAT 4 potentiostat (AMETEK, Cassatt Road Berwyn, PA, USA) was employed to apply a 10 V voltage across these electrodes, enabling an examination of how the fillers contributed to the conductivity behavior of the composite coatings. The 10 V were applied for a time equal to 600 s, useful for allowing the system to settle around a stable current value measured between the two electrodes applied to the surface of the coating. The measurement setup is schematized in Fig. 1a. In contrast, Fig. 1b illustrates the procedure employed to assess the magnetic characteristics of the coatings. This involved placing a magnet with a 1 cm^2 surface area, connected to weights of varying magnitudes, onto an analytical balance. Following this, the sample was gradually approached to the magnet to measure the attractiveness of the paint. The maximum weight lifted was then quantified in N/m^2, representing the magnetic force exerted by the sample.

3. Results and discussion

3.1. Additives and coatings morphology

Fig. 2a, acquired with SEM, displays the morphology of stainless steel flakes, which exhibit a combination of regular and more irregular, jagged shapes. Concerning the dimensional assessment of the filler, the flakes are consistently less than 60 μm in width and possess a very small thickness, measuring less than 1 μm, as emphasized in the magnification of the figure. In contrast, magnetite powders exhibit markedly distinct structures and dimensional variations, as depicted in Fig. 2b. These granules possess a three-dimensional morphology, characterized by considerable irregularity and a wide range of sizes. Within this spectrum, it is possible to observe very fine powders at the micrometer scale, as well as much larger granules, approximately 50 μm in size. Nevertheless, both types of fillers have dimensions that are suitable for spray applications in the development of protective wood coatings.

As a result, the two additives were employed as versatile wood pigments through their incorporation into a commercial acrylic paint. Fig. 3 illustrates both the cross-sectional view (on the left) and the top-view appearance (on the right) of the three series of samples under investigation. Fig. 3a, which pertains to the reference sample REF, demonstrates that the commercial paint yields uniform coatings with consistent thickness and minimal defects. The incorporation of a substantial amount of flakes, on the other hand, results in significant alterations in the morphology of the coating, as depicted in Fig. 3b. The cross-sectional view of the layer reveals a pronounced presence of flakes, primarily

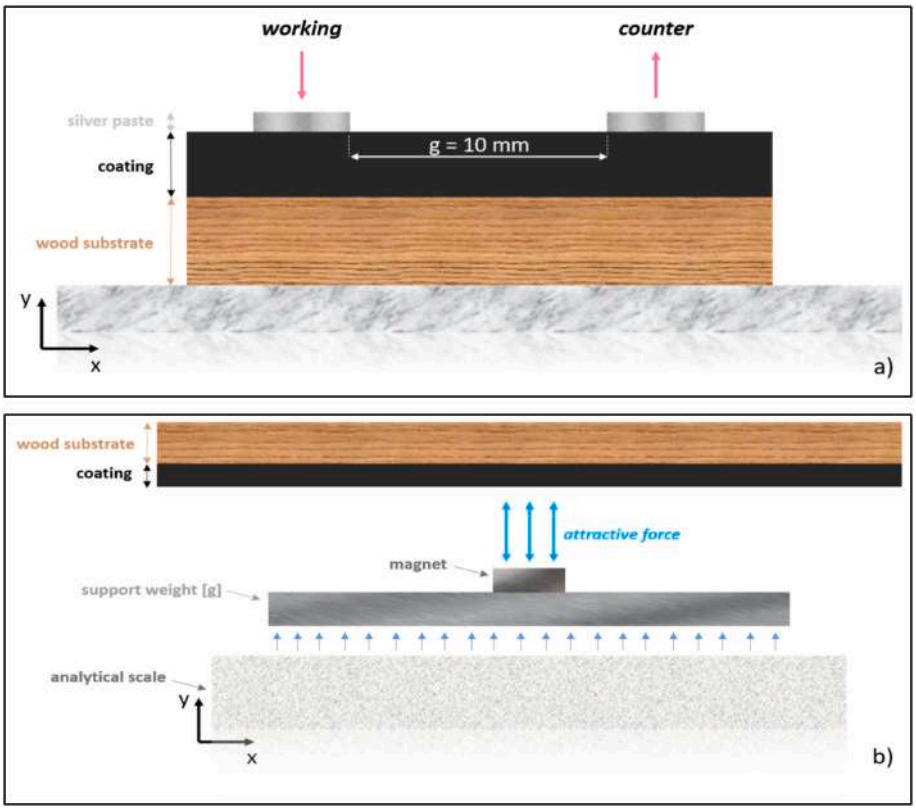

Fig. 1. Measurement setup [cross view] for a) conductivity and b) for magnetic attraction of composite coatings.

oriented in a parallel direction to the wooden substrate. This phenomenon could be attributed to the settling of the flakes during the curing process of the polymer matrix. The release of moisture may induce the reorientation of the filler and contribute to an increase in the overall compactness of the layer. A similar occurrence, albeit with lesser extent, had been previously noted in a prior study focused on the utilization of stainless steel flakes in wood coatings [65]. The top-view depiction of the sample, as shown in Fig. 3b, illustrates that the flakes are predominantly oriented parallel in relation to the coating's surface, thereby corroborating their arrangement within the polymer matrix observed in the cross-sectional view. Fig. 3c, on the other hand, exhibits a distinct behavior of the magnetite powders. Despite their uniform dispersion throughout the coating, as further affirmed by the top-view image in Fig. 3c, the granules demonstrate a specific pattern. The larger particles, indeed, are primarily found at the bottom of the coating in contact with the substrate but are also present in the middle of the layer itself. This occurrence can be attributed to the substantial weight of the magnetite, leading to the settling of the larger particles during the polymer matrix curing process, which took place by arranging the samples in a flat position. Consequently, the two "lines" formed by the larger granules, one at the bottom and the other in the middle of the coating, highlight the two layers formed as a result of the dual depositions of the composite paint. Moreover, the incorporation of magnetite results in the formation of a coating with a thickness that expands from approximately 180-190 μm in samples REF and SSF to around 250 μm in sample MAG. This is due to the substantial increase in the volume of deposited material caused by the presence of the larger granules. Hence, the filler not only changes the morphological characteristics of the coating but also modifies its dimensions, indicating a noteworthy influence on the protective attributes of the acrylic matrix. Nonetheless, it is quite encouraging to note the substantial presence of both flakes and magnetite granules within the coating section. To examine the internal structure of the coatings, the samples underwent a brittle fracture process in liquid nitrogen. Despite the destructive nature of this procedure, both types of fillers remained firmly adhered to the coating, indicating excellent compatibility with the acrylic matrix.

To assess the visual impact of the fillers, colorimetric measurements were conducted on the samples, determining the color change ΔE in comparison to the REF coating, which consists solely of the acrylic matrix. ΔE was computed in accordance with the ASTM E308-18 standard [66]:

$$\Delta E = \left[(\Delta L^*)^2 + (\Delta a^*)^2 + (\Delta b^*)^2\right]^{1/2}$$

where, L*, a*, and b* represent the colorimetric parameters for brightness (ranging from 0 for black to 100 for white objects), the red-green axis (positive values indicate red, while negative values indicate green), and the yellow-blue axis (positive values correspond to yellow, while negative values correspond to blue), respectively. Table 2 displays the measurements of the three coordinates L*, a*, and b* obtained for each individual series of samples, along with the calculated ΔE in comparison to the reference sample REF. To gain insight into how the samples look, it is possible to consult the image provided in Fig. 7. Incorporating flakes into the paint, and even more prominently, adding magnetite granules, results in a noticeable darkening of the coating, as indicated by the decline in L* values. This effect is linked to the reduction of b* towards neutral values, causing the disappearance of the underlying wood's yellowish tone. Essentially, both fillers contribute to the opacity of the acrylic matrix, introducing distinct colors to the layer. In particular, the flakes introduce a metallic sheen and a grayish hue to the coating, while the MAG sample exhibits a deep black appearance. These effects result in a highly pronounced alteration in color ΔE when compared to the REF sample, amounting to roughly 30 points for the SSF sample and 66 points for the MAG sample. These two values hold significant relevance, particularly when taking into account that the human eye can discern color variations ΔE of approximately 1 unit [67,68]. Similarly, the addition of the two fillers to the acrylic matrix leads to a reduction in gloss (Table 2), which drops to values of approximately 11

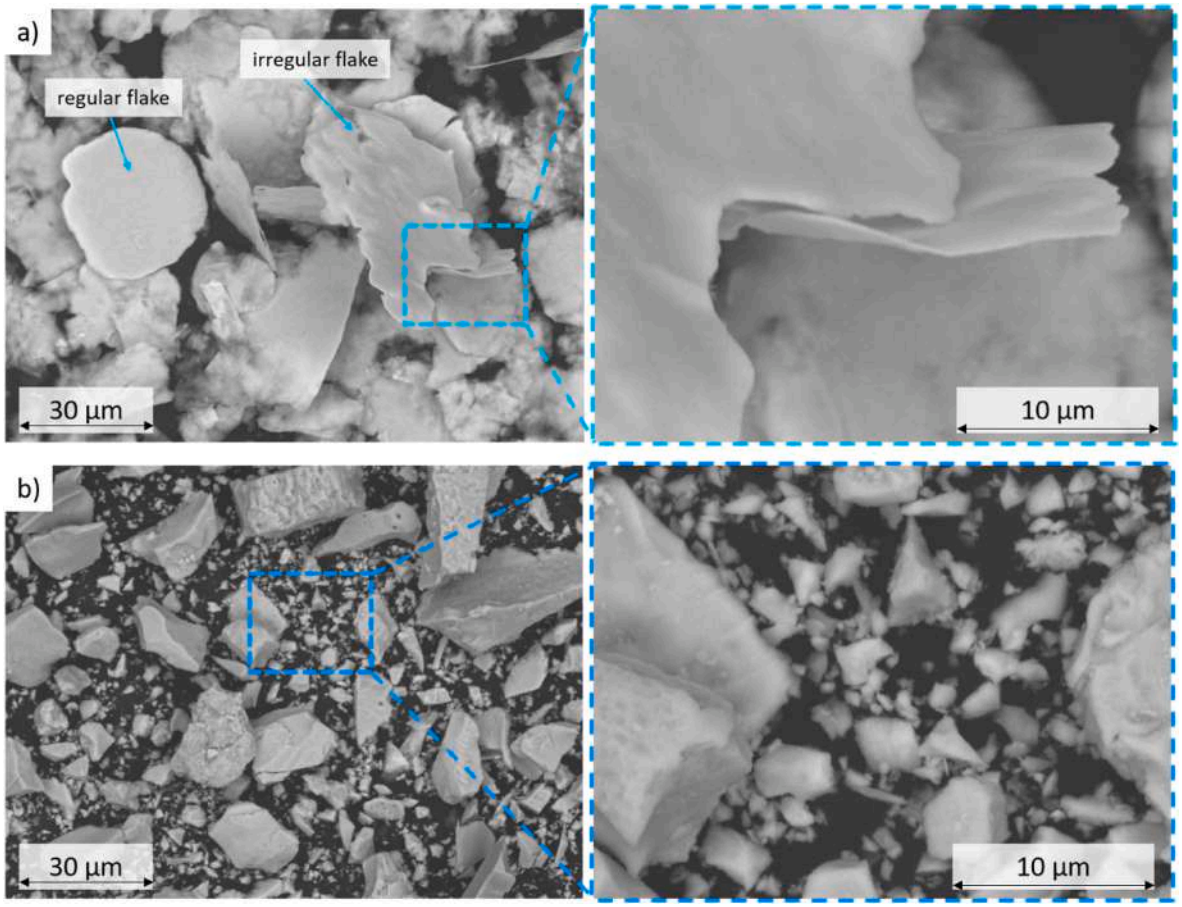

Fig. 2. SEM micrographs of a) the stainless steel flakes and b) the magnetite powder.

and 21 for samples SSF and MAG, respectively.

As a result, it is feasible to ascribe a vivid color transformations to the two fillers, which can associate them to standard commercial pigments. Additionally, the two additives affect the paint's reflective properties, as indicated by the decrease in gloss. Alongside their significant influence on the visual characteristics of the coatings, the two fillers introduce notable alterations in the composite layer's structure, yet without causing substantial defectiveness.

3.2. Durability of the coatings in aggressive environments

Both the stainless steel flakes and magnetite powder play distinct roles in altering the visual characteristics of wood paint. However, to ascertain whether these fillers influence the paint's long-term durability, all three sample series underwent accelerated degradation assessments, including Xenon arc light exposure and climatic chamber exposure tests.

In recent research, the impact of functional fillers and bio-based pigments on the protective properties of wood paints has been explored [65,69–72]. These investigations involved the assessment of paint degradation through accelerated degradation tests, which included exposure to UV-B and UV-A radiations. These tests were accompanied by infrared spectroscopy FTIR analysis. However, it's worth noting that this analysis method proved ineffective in revealing specific phenomena induced by the degradation tests, mainly due to the robust UV resistance of acrylic paint. Moreover, the detection of inorganic fillers like stainless steel flakes and magnetite powders proves challenging through infrared analysis. Hence, the potential degradation of the samples in this research was assessed using straightforward colorimetric and gloss analyses. In addition, to produce a more realistic simulation of solar radiation exposure, the samples underwent accelerated testing utilizing xenon lamps, instead of the more aggressive yet less representative UV-A and UV-B radiation.

Fig. 4a illustrates the change in color ΔE observed throughout the accelerated degradation test of the three samples. It is compared to the behavior of the wooden panel, which serves as an additional reference to underscore the protective function of the paint. The poplar wood exhibits a significant and immediate alteration in color, primarily attributed to the rapid degradation of its primary constituents, namely cellulose, hemicellulose, and lignin, associated to a noticeable yellowing of the sample. Although the degradation process is equally swift, sample REF experiences less pronounced changes in color, amounting to approximately 5 points. The acrylic paint, in fact, acts to decelerate the deterioration of the wooden substrate and remains resilient to the impact of aggressive radiation due to its inherent durability [73,74]. Indeed, the ΔE of 5 points observed in Sample REF, indicating a mild yellowing, primarily results from the degradation of the underlying wood rather than any chemical deterioration of the coating. This conclusion finds support in a recent investigation [36], which has empirically demonstrated that transparent acrylic wood paints do not manifest aesthetic changes when applied to surfaces that do not undergo color alterations upon exposure to UV radiation. Consequently, the paint can only offer partial mitigation of wood deterioration phenomena. Furthermore, owing to the paint's transparency, any color shift induced by the xenon lamp radiation in the wood substrate remains visible. Conversely, the incorporation of steel flakes appears to mask these degradation effects. Importantly, the durability of this material remains unaltered even when exposed to UV radiation, as noted in prior research [75]. Additionally, the flakes contribute to shielding by partially reflecting the ultraviolet radiation [76]. Likewise, sample MAG demonstrates hardly any noticeable alteration in color due to its strong

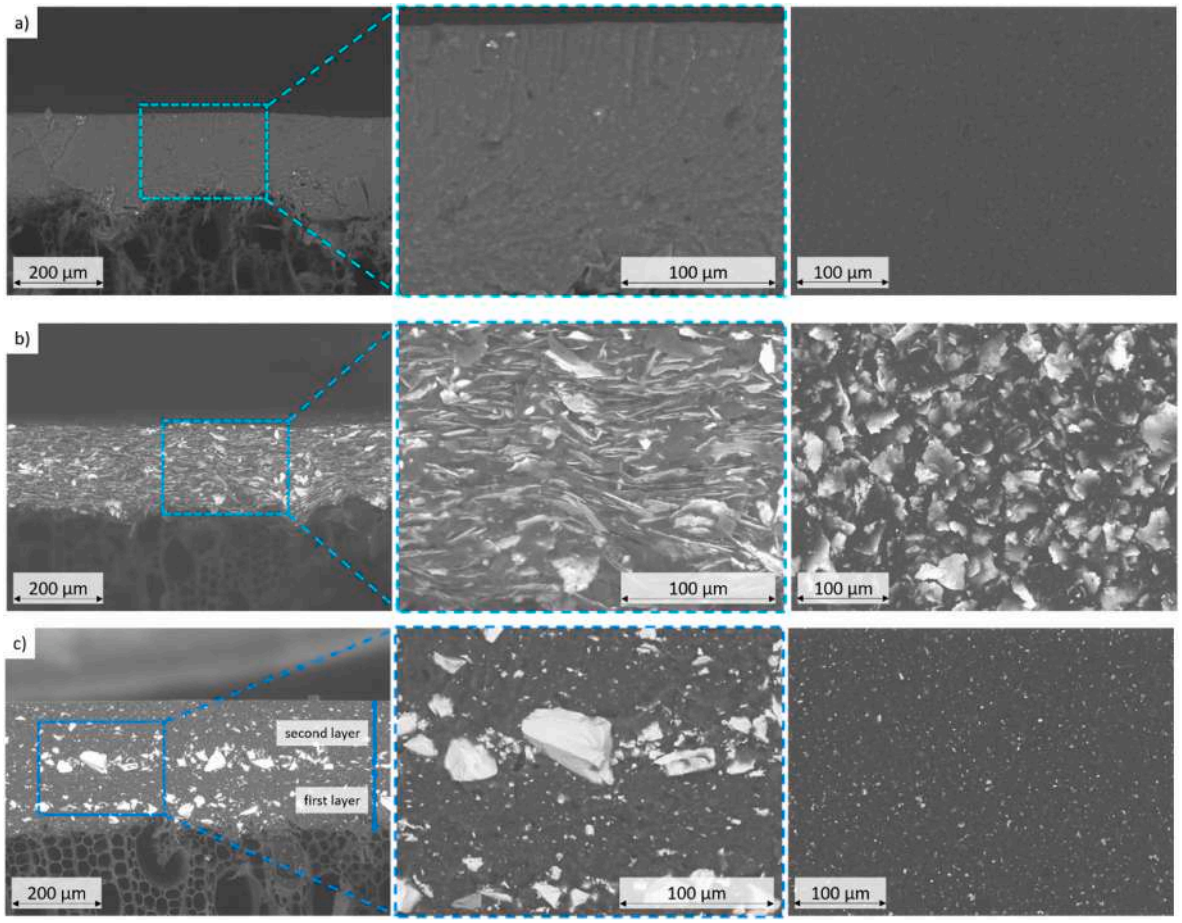

Fig. 3. SEM micrographs of the cross-section (on the left) and top-view optical microscope micrographs (on the right) of a) sample REF, b) sample SSF, and c) sample MAG.

Table 2
Results of the colorimetric and gloss measurements.

Sample	L*	a*	b*	ΔE (respect to sample REF)	Gloss (60°)
REF	88.63	0.28	18.01	0.00	30.8
SSF	63.84	0.25	1.73	29.66	11.1
MAG	25.1	0.54	0.02	66.03	21.0

resistance to UV radiation, a quality previously utilized in scientific literature to safeguard vulnerable substrates from photochemical deterioration [77]. Ultimately, both the flakes and the magnetite offer the benefit of concealing any undesirable aesthetic problems arising from wood degradation due to their high covering ability, which resembles that of other fillers that impart a dark color to the paint [69].

Regardless, the gloss measurements (depicted in Fig. 4b) do not emphasize any potential degradation phenomenon, primarily linked to the wooden base, as they reveal minimal fluctuations throughout the accelerated test. In conclusion, the acrylic paint demonstrates

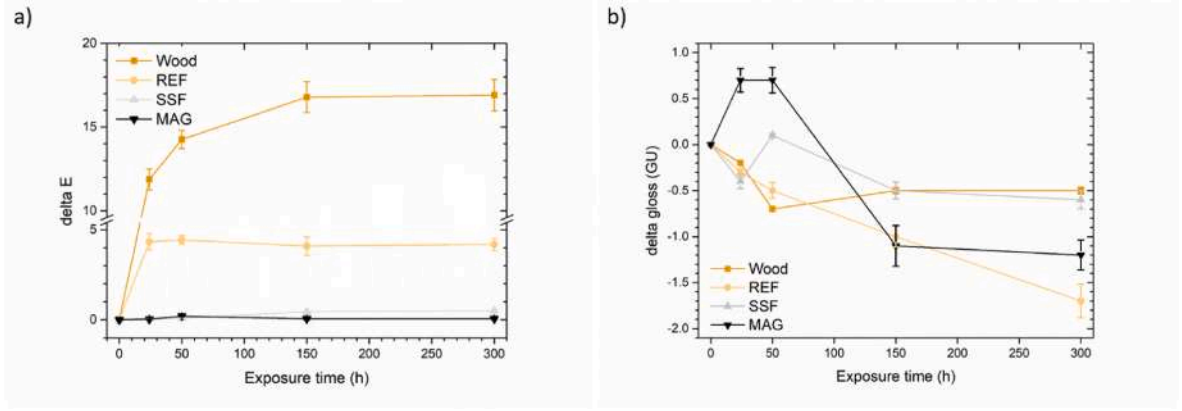

Fig. 4. Evolution of a) color and b) gloss of the samples during Xenon exposure test. (For interpretation of the references to color in this figure legend, the reader is referred to the Web version of this article.)

commendable chemical resistance to Xenon light, effectively retarding the photo-oxidation degradation of the wooden substrate to some extent. However, the paint's transparency does expose the yellowing of the wood. On the other hand, both the steel flakes and magnetite powders exhibit resilience to the accelerated degradation test, partially mitigating UV radiation, and thus preserving the visual appeal of the sample. Consequently, the durability and color-preserving attributes of the functional pigment remain intact for outdoor applications, even when the painted component is directly exposed to solar radiation.

As per the evaluation criteria presented in Table 3, the assessment of sample performance during the climatic chamber exposure test is based on the extent of crack formation and the potential occurrence of whitening phenomena, as stipulated by the UNI 9429 standard [56].

Due to their vulnerability to low temperatures and their susceptibility to moisture penetration through their inherent bulk porosity, organic coatings are often prone to sudden temperature fluctuations. Such occurrences can lead to the formation of fissures in the coating [36,69], potentially compromising the polymer layer's ability to effectively safeguard the underlying substrate. Consequently, the assessment of crack development is a critical aspect when evaluating coating performance under thermal stress. In this regard, the three sample series yielded positive results, as the respective coatings did not exhibit noticeable cracks. As per the standard guidelines, all three layers fall within category 0, signifying that no imperfections were detected through 4x optical microscope inspections. Therefore, irrespective of the type of filler integrated into the coating, it can be confidently stated that both the stainless steel flakes and the magnetite powder do not induce any structural distortions in the polymeric matrix due to thermal stress. Furthermore, the three categories of samples also display a favorable behavior with respect to the constancy of their appearance, akin to the classification of "cracks". Fig. 5 depicts the progression of the overall color variability, ΔE, as the outcome of five colorimetric assessments conducted for each sample, with three samples in each set (resulting in a total of 15 measurements per set). All three samples show a color change so low that it can be considered negligible for testing purposes. Furthermore, this chromatic stability seems to be enhanced by the addition of flakes, but especially by magnetite. This phenomenon is closely related to the dark shades imparted by the two fillers, which mask potential whitening phenomena (already very limited in the polymer matrix of the reference sample REF). Indeed, the rise in the L* value is insignificant (less than 1 unit), indicating imperceptible whitening effects.

Lastly, the cross-cut test was executed on the samples before and after their exposure in the climatic chamber to investigate whether the accelerated degradation test had induced any issues regarding the adhesion between the coatings and the wooden substrate. Fig. 6 shows the test results, which highlight excellent performance of all three types of coatings, whose adhesion does not appear to be negatively affected by the thermal shocks they have been subjected to. In accordance with the ASTM D3359-17 standard [57], all the specimens unmistakably demonstrate a grade 5B, the most superior, regarding adhesion, with no observable coating detachment. Consequently, both the flakes and the magnetite powder illustrate that they do not induce noticeable flaws in the polymer matrix of the coating, nor do they promote moisture absorption in the composite film. This preserves the strong adhesion of the

Table 3
Classification of crack formation and whitening as a result of exposure in the climatic chamber.

Category	Cracks	Whitening
0	No alterations	No whitening
1	Defectiveness discernible exclusively with 4x optical system	Light whitening
2	Evident cracks or breaks	High whitening

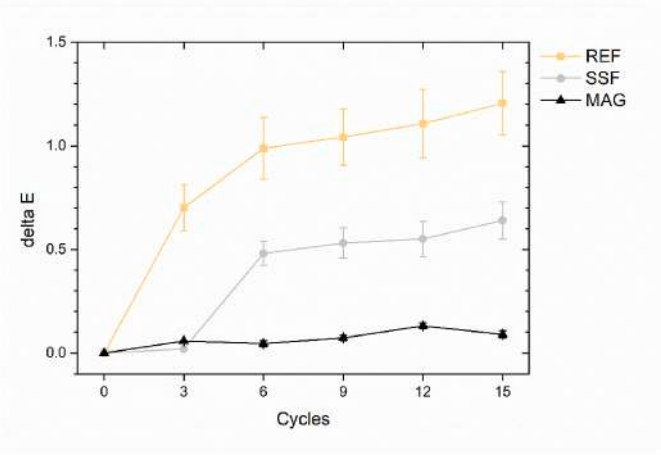

Fig. 5. Alteration in color of the samples under climatic chamber conditions. (For interpretation of the references to color in this figure legend, the reader is referred to the Web version of this article.)

layer, even following repeated thermal stresses.

In summary, all the test samples demonstrate remarkable resilience to extended temperature fluctuations, with the coatings showing only minimal whitening and fracture development. These results can be attributed to the excellent adhesion stability of the coatings, which remains unaltered during the accelerated degradation test. The introduction of both filler types, known for their durability under thermal stress, has no impact on the protective qualities of the acrylic paint. Clearly, both the stainless steel flakes and the magnetite powder could be utilized in outdoor coatings for areas subject to substantial temperature fluctuations.

3.3. Coatings liquid resistance

The liquid resistance test is a common procedure aimed at acquiring pertinent data regarding the protective attributes of wood coatings and the potential consequences of pigments [38,78] and additives [70,79] integrated into the paint formulation. The appearance of the coatings after testing is depicted in Fig. 7. Upon closer inspection of the image, it becomes evident that the three sets of samples display varying behaviors. In general, the solutions containing NaCl, ethanol, and detergent have a minimal impact on the visual aspect of the coatings, while the presence of red ink significantly alters the overall appearance of the samples.

Hence, colorimetric analyses were carried out to more precisely determine the extent of sample discoloration upon exposure to the designated test solutions. Fig. 8 illustrates the measurement outcomes, emphasizing the pattern previously noted in Fig. 7. The solutions containing NaCl, ethanol, and detergent induce only minor alterations in the samples' appearance, registering within the range of 0–1. The acrylic paint (sample REF) demonstrates exceptional chemical resistance, seemingly impervious to the filler's influence. In fact, the overall ΔE values are remarkably limited, underscoring the composite coatings' capacity to provide effective insulation, even when incorporating substantial quantities of stainless steel flakes and magnetite powders. However, it's worth mentioning that the aesthetics of the coatings are noticeably affected by red ink, leading to uniform color modifications ranging from grade 3 to 5 in all three coatings. This outcome was expected, given red ink's potent coloring properties and its easy absorption into the polymeric matrix of paints, as previously indicated in other literature studies [70–72]. Indeed, the acrylic matrix readily assimilates the red ink, leading to pronounced coloration in sample REF. However, the presence of stainless steel flakes substantially curtails this effect, reducing the degree of discoloration from 5 to 3. This outcome can also

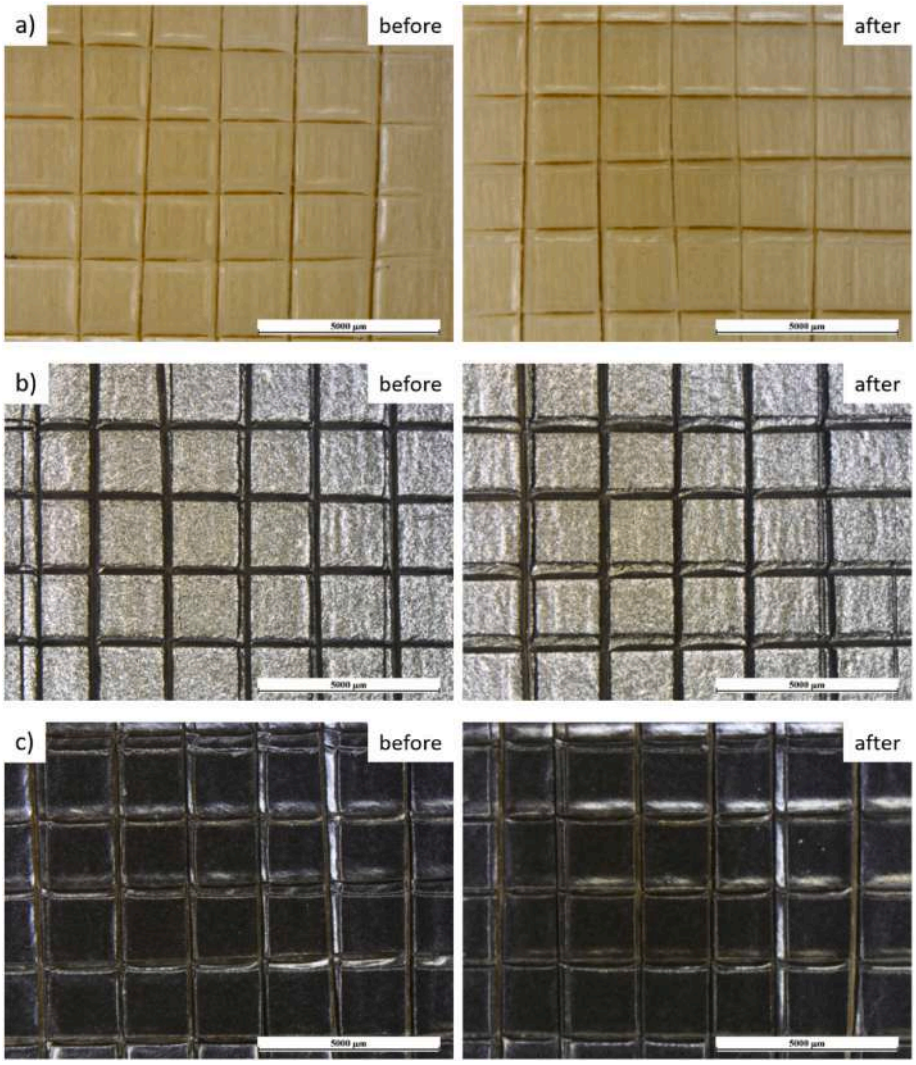

Fig. 6. Cross cut test results before and after exposure into the climatic chamber of a) sample REF, b) sample SSF and c)sample MAG, observed with optical microscope.

be attributed to the initially darker base color, which effectively masks the color alteration brought about by the ink. On the other hand, despite the robust black base color of sample MAG, its interaction with red ink results in a noticeable yellowing of the coating, leading to a color shift of grade 5. Therefore, the initial shade of the sample does have some influence on its resistance to liquids. However, it is essential for the filler to play a role in terms of creating a barrier against solution absorption. In this scenario, the compactly distributed flakes oriented parallel to the coating's surface work to reduce ink absorption, while the magnetite granules introduce discontinuities within the acrylic matrix, allowing for the percolation of the test solution.

Nonetheless, the liquid resistance test provides solely qualitative insights, primarily related to the color alterations in the coatings. Consequently, to assess the actual quantitative impact of incorporating stainless steel flakes and magnetite powder on the coatings' barrier properties, the samples were additionally exposed to the liquid water uptake test, monitoring the water absorption of the coatings. Fig. 9 illustrates the evolution of water absorption observed in the experiment. All three sample groups demonstrate a comparable pattern, initially showing substantial liquid intake. As the experiment progresses, the rate of water absorption by the coatings gradually diminishes. This represents a typical trend of wood coatings, already observed in previous literature works [70,72,81]. Despite a very similar trend, the graph highlights slight differences among the outcomes of the three samples, consistent with the results of the liquid resistance test expressed in Fig. 8: the flakes, rather than the magnetite, exert a slight barrier effect on the solution absorption within the coating, as indicated by the lower water uptake values of sample SSF. The reduction in water uptake compared to the reference sample REF, approximately 11.5 %, highlights the protective contribution of the flakes, as already indicated by the reduced color change upon contact with the red ink. Once again, the specific 2D structure of the flakes and their partial orientation within the coating play a crucial role in influencing the performance of the acrylic matrix.

In summary, the stainless steel flakes exhibit a notable reinforcing influence on the acrylic matrix's barrier properties within the coating, surpassing the impact of magnetite powder. More precisely, they express the ability to partially mitigate the color changes induced by aggressive solutions when they come into contact with the composite layer, thereby decreasing their absorption. As a result, the findings endorse the incorporation of such additives as functional pigments for outdoor applications, where coatings may be exposed to external agents, such as aggressive liquids.

3.4. Coatings multifunctional features

In the modern paint market, there is a shift away from the mere need for protective and visually appealing coatings. Instead, there is a

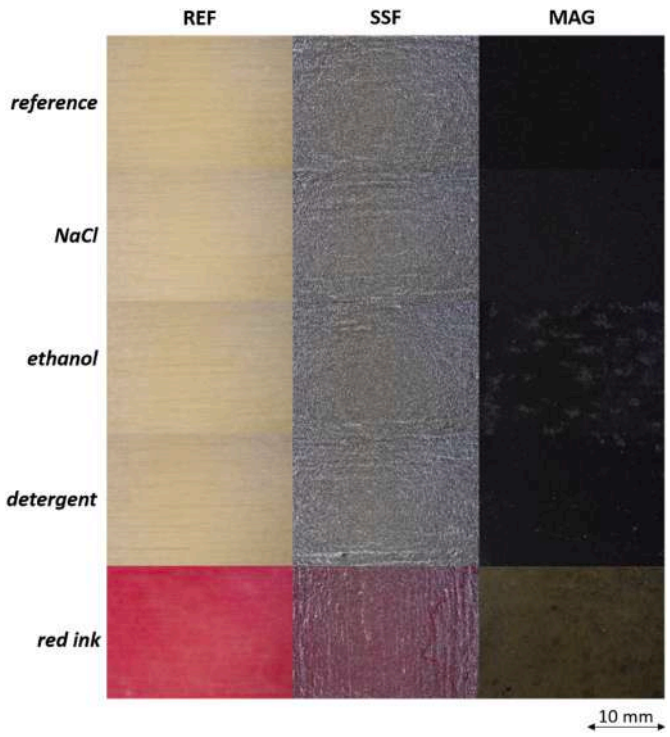

Fig. 7. Change of the appearance of the samples after the liquid resistance test. Indeed, the assessment of test results relies on gauging the extent of color change resulting from the interaction between the coating and the test solutions, as indicated by the sources cited in Table 4 [80]. (For interpretation of the references to color in this figure legend, the reader is referred to the Web version of this article.)

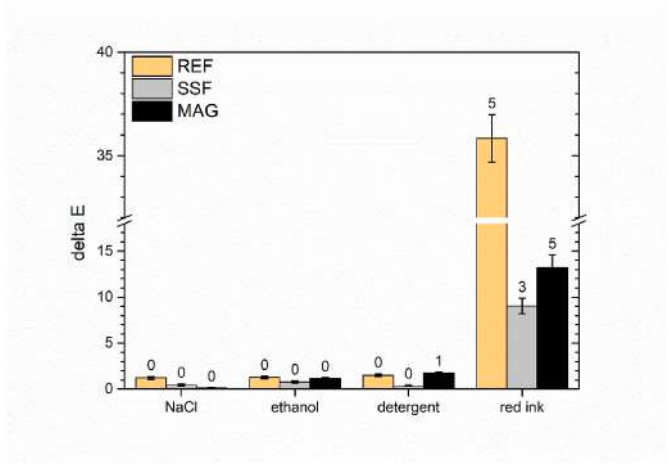

Fig. 8. Color variation of the samples after the liquid resistance test. The numbers displayed above the columns reflects the discoloration levels detailed in Table 4. (For interpretation of the references to color in this figure legend, the reader is referred to the Web version of this article.)

growing demand for multifunctional coatings that can encompass additional properties suitable for various technological applications. Keeping this objective in view, the samples underwent several characterization tests to explore the multifaceted role of the chosen additives.

3.4.1. Coatings hardness and abrasion resistance

Fig. 10 provides a visual illustration of the marks created by the indenter on the surface of the three coatings. While these three images might seem quite alike, the behavior of sample SSF (Fig. 10b) actually

Table 4
Values indicating color alteration in correspondence with the degree of fading.

Level	Degree of Discoloration	Color Difference
0	no color change	≤1.5
1	very slight fading	1.6-3.0
2	subtle alteration in color	3.1–6.0
3	visible discoloration	6.1–9.0
4	drastic fading	9.1–12.0
5	total loss of color	>12.0

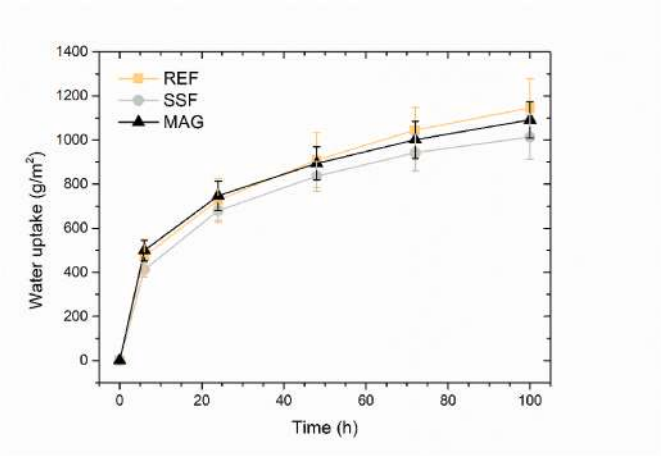

Fig. 9. Monitoring of the water uptake by the coatings.

diverges from the other two samples under investigation. Specifically, the length of the indentation is notably reduced, indicating an enhanced hardness in the acrylic matrix due to the presence of stainless steel flakes.

Fig. 11 better evidence this behavior, depicting the outcome of measurements of the Buchholz hardness test, with the average length of the impressions made by the instrument's indenter device corresponding to the Buchholz hardness value. The acrylic matrix exhibits notable less hardness, making it susceptible to indenter penetration. As a result, the recorded hardness values are quite low, averaging less than 50 on the Buchholz scale. Conversely, the incorporation of flakes leads to a significant 14.7 % reduction in the average notch length, resulting in an increase in hardness to a value of 50. In the end, stainless steel flakes are acknowledged for their favorable mechanical characteristics. A recent study concluded that this filler enhances the hardness of even an aluminum matrix, functioning as a rigid supporting component [82]. Additionally, prior research has successfully shown that even minor additions of flakes can bring about a substantial enhancement in the hardness of acrylic paints [65]. Otherwise, the impact of magnetite is less pronounced, with sample MAG revealing a modest 5.0 % increment in the hardness of the acrylic matrix. Despite the greater hardness of magnetite relative to the acrylic matrix, the tiny granules located near the surface are incapable of exerting a substantial influence on the coating's hardness attributes.

Nonetheless, the mechanical properties of magnetite and its favorable compatibility with the acrylic matrix influence the coating's resistance to abrasion. The pattern of mass reduction in the three coatings throughout the Taber test is illustrated in Fig. 12. The trend of mass loss displays an almost linear progression over the course of the test, with variations occurring in the steepness of the curves for the three samples. The introduction of stainless steel flakes, and particularly magnetite powder, leads to a decrease in mass loss during the abrasion procedure. After 3000 Taber cycles, samples SSF and MAG exhibit a reduction in mass loss by 9.6 % and 26.1 %, respectively, in comparison to the pure acrylic matrix (REF sample).

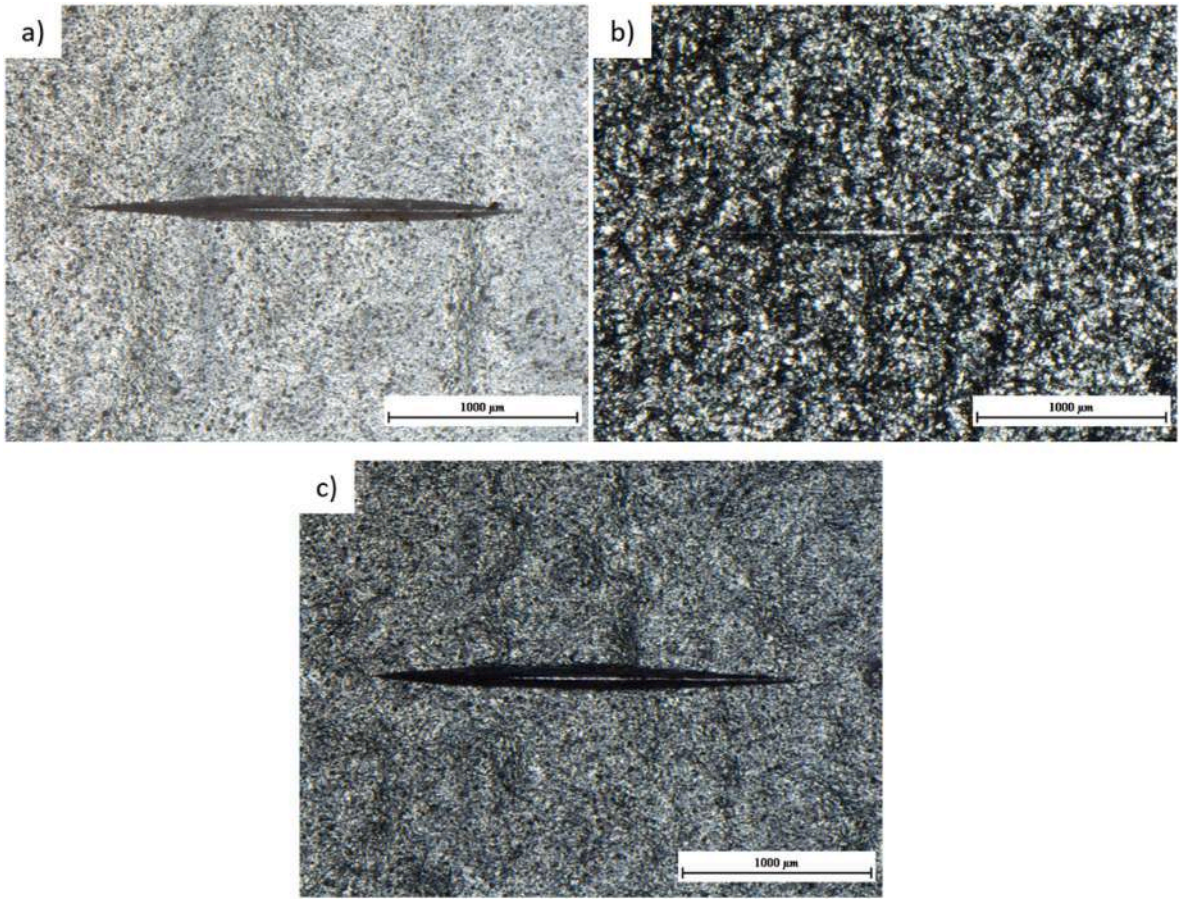

Fig. 10. Optical microscope images of Buchholz test notches on a) sample REF, b) sample SSF and c) sample MAG.

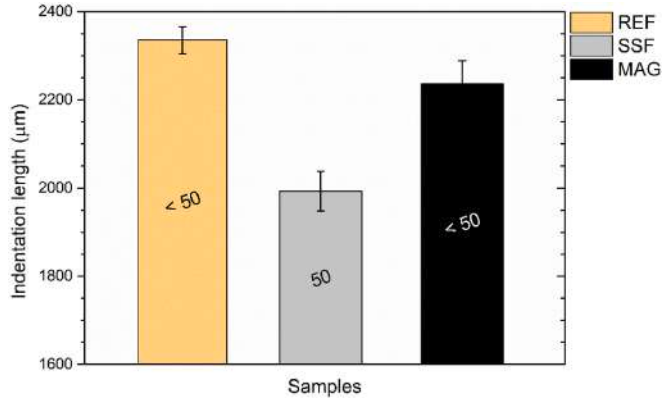

Fig. 11. Average length of indentation marks in Buchholz hardness testing, alongside their respective Buchholz hardness results.

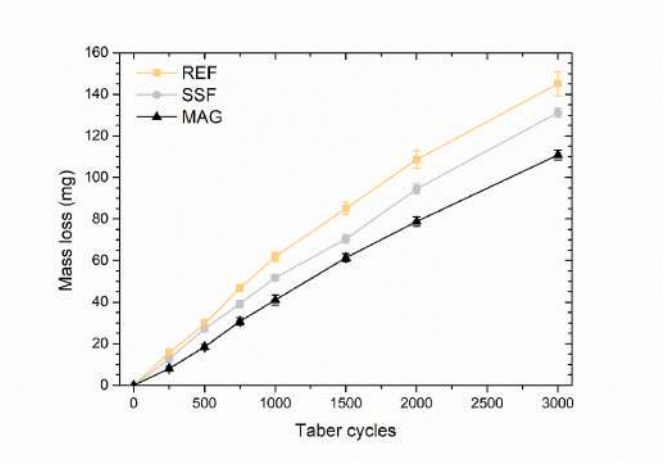

Fig. 12. Coatings mass loss, as a function of the Taber cycles.

Nonetheless, when evaluating the performance of the three samples, it's important to consider the varying densities of their respective coatings. The acrylic matrix possesses a specific weight that ranges from 1.01 to 1.18 g/cm^3, whereas stainless steel flakes and magnetite powders have different bulk densities of about 0.2–0.4 g/cm^3 and approximately 5.10–5.20 g/cm^3, respectively. As a result, due to the distinct volumes associated with the same mass loss, the samples were subjected to a profile analysis of the imprint created after 3000 Taber cycles to more effectively emphasize the extent of the abrasion process. An illustration of these measurements, demonstrating the behavior of all three samples, is presented in Fig. 13. The graph illustrates a decrease in the imprint depth in the SSF and MAG samples, amounting to roughly 4–5 µm, corresponding to an enhancement of around 20 %. As a result, the analyses emphasize the efficient enhancement brought about by the two fillers, significantly diminishing the effects of the coating's abrasion process.

Because the abrasion profiles of the SSF and MAG samples are similar, yet they display distinct mass loss behaviours in the Taber test, it can be concluded that the inclusion of these two fillers does not considerably change the ultimate density of the coating. Thus, the varied mass removal during the abrasive process is not attributed to differing filler densities, but rather to their distinct protective performances.

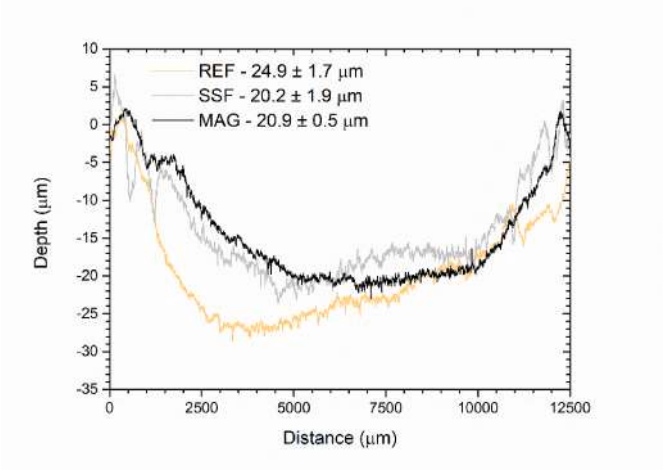

Fig. 13. Profile analysis of the footprint generated following 3000 Taber cycles. The values in the legend correspond to the mean maximum depth calculated from 50 measurements for each series (comprising 10 measurements for 5 samples).

Thus, for a more in-depth examination of the reinforcement mechanism enacted by these fillers, SEM analysis was performed on the samples after the Taber test. Fig. 14 displays the impression created by the Taber grinding wheels observed with the optical microscope (left) and a closer examination of the damage morphology scrutinized using SEM (right). The impression is readily visible when examined through the optical microscope, a result of the notably intense abrasive action induced by the Taber test. Nevertheless, the most valuable insights are obtained from SEM examinations. In sample REF (Fig. 14a), the acrylic matrix displays the characteristic abrasion marks left by the Taber grinding wheels, showcasing a consistent erosive pattern along the entire path. Even the surfaces of the stainless steel flakes (Fig. 14b) exhibit evidence of the abrasive wheel's movement. Despite the rigorous abrasion and the shear forces they endure, numerous flakes remain undamaged, showcasing their impressive resilience. The horizontally oriented flakes serve as a sliding surface for the grinding wheel, thereby mitigating its abrasive impact. Conversely, flakes that deviate from perfect parallel alignment with the coating plane undergo plastic deformation, consequently dissipating the abrasive energy of the grinding wheel. Indeed, a recent investigation [44] delved into the influence of these flakes on porcelain enamel coatings, unveiling the remarkable protective benefits brought about by the filler. The flakes experienced instances of plastic deformation resulting from the abrasive process, as outlined in the study. The prior research, which explored the impact of varying concentrations of stainless steel flakes, underscored the valuable protective role played by this filler [65]. This flakes not only exhibit strong compatibility with the acrylic matrix but also effectively disperse energy through plastic deformation, contributing to their excellent protective properties. Lastly, also the magnetite granules exhibit a capability to reduce the abrasive effects of the Taber grinding wheels (Fig. 14c). In this instance, their protective role is attributed to the inherently brittle nature of the granules. The larger granules tend to fracture under the abrasive action, producing micro-dust particles that provide increased resistance to the grinding wheel's movement. Additionally, a significant number of these resultant by-products tend to fill the defects generated within the polymer matrix, as depicted in the figure, enhancing the stability and shear stress resistance of the coating.

In summary, the stainless steel flakes and magnetite powder both

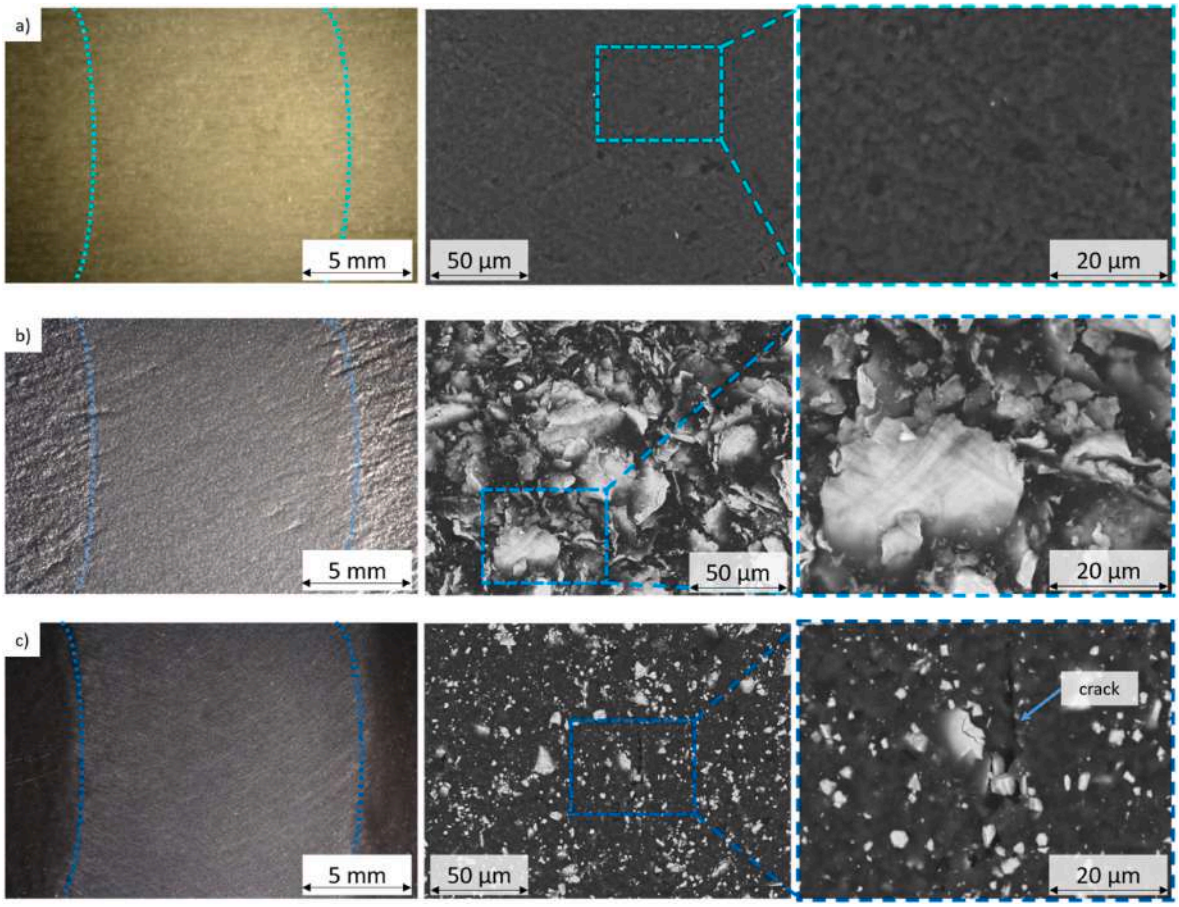

Fig. 14. Optical microscope (on the left) and SEM micrographs (on the right) of a) sample REF, b) sample SSF, and c) sample MAG, after 3000 Taber cycles.

offer a practical protective effect, diminishing the mass loss resulting from abrasion occurrences. These additives go beyond serving a purely aesthetic role as alternative pigment sources; they also have the capacity to bolster the mechanical characteristics of the acrylic matrix while preserving the coating's long-term durability.

3.4.2. Coatings electrical conductivity and magnetic properties

Due to the substantially higher electrical conductivity of both the stainless steel flakes and magnetite powders compared to the polymeric matrix, the primary focus of the study was to explore how these two fillers assist in decreasing the coating's electrical resistivity. Several studies have indeed shown a tangible conductive impact of these materials when integrated into polymeric matrices [83,84]. Fig. 15 shows the output of the potentiostatic measurements, carried out by applying the setup described in Fig. 1a. The picture underscores a notable contrast in the performance of sample SSF when compared to the other two samples being studied. In sample REF, the acrylic matrix displays relatively low measured current values, which are characteristic of polymeric materials that can be considered as electrical insulators. In contrast, the incorporation of stainless steel flakes leads to a substantial increase in the current by over three orders of magnitude. However, despite its good conductivity at room temperature [85], magnetite does not yield a significant impact, as the outcome in sample MAG is similar to that of sample REF. These outcomes can be readily explained by examining the structural morphology of the coatings, as depicted in Fig. 3. The closely packed flakes provide a straightforward path for the current to traverse within the acrylic matrix of the coating. In contrast, although magnetite powders are uniformly dispersed throughout the layers, they often lack direct contact with one another, thus failing to reach the percolation threshold required to significantly alter the polymer's conductivity characteristics. This factor becomes even more significant when taking into account that the larger powder particles do not reside on the coating's surface. Instead, as observed in SEM cross-section examinations, they tend to accumulate at the lowermost part of each individual layer.

Table 5 provides an overview of the resistivity values recorded in the conductivity tests. The surface resistance R_s was determined by using the applied voltage V and the measured current I, following Ohm's law. Subsequently, the surface resistivity ρ_s was calculated in accordance with the formula prescribed in the standard [62]:

$$\rho_s = \frac{P}{g} R_s$$

where P represents the effective perimeter of the guarded electrodes, while g is the distance between the two electrodes. Through the process of standardizing the surface resistivity results in relation to the measurement for the REF reference sample, it becomes feasible to underscore the substantial impact of the two fillers on altering the electrical conductivity characteristics of the acrylic matrix. The inclusion of stainless steel flakes leads to a reduction in the surface resistivity of the coating by more than three orders of magnitude, whereas the contribution of magnetite, as mentioned earlier, remains insignificant.

Table 5
Surface resistivity measurements.

Sample	Voltage applied V [V]	Current measured I [A]	Surface Resistance R_s [Ω]	Surface Resistivity ρ_s [Ω]	Surface Resistivity normalized/
REF	10	6.73E-9	1.49E9	3.72E10	1.00
SSF	10	1.40E-5	7.16E5	1.79E7	4.82E-4
MAG	10	4.42E-9	2.26E9	5.65E10	1.52

Magnetite is well-known for its distinctive magnetic properties. Indeed, various recent studies in the literature have emphasized the potential to achieve favorable magnetic properties in polymer matrix composites through the incorporation of magnetite powders [86,87]. Similarly, stainless steel flakes also exhibit intriguing magnetic attraction characteristics, exploitable in polymeric matrices [88,89]. Hence, the evaluation of how these two fillers contribute to rendering the paint magnetic was conducted using the configuration outlined in Fig. 1b, analyzing the magnetic attractive force of the two composite coatings. The graph in Fig. 16 underscores a distinct contrast in the behavior exhibited by the two composite coatings. Notably, sample SSF demonstrates a magnetic attractive force approximately five times greater than that of sample MAG, even though both coatings contain the same wt.% of magnetic filler. Similar to the conductivity characteristics, the rationale behind this outcome is rooted in the coating's morphology, rather than the inherent attributes of the two fillers. The flakes, in fact, are predominantly oriented and tightly packed within the coating matrix, with concentrated clusters near the outer surface of the composite layer. In contrast, the larger magnetite granules tend to settle as the coating cures, positioning themselves at the bottom of the respective depositions. Consequently, the surface of coating SSF benefits from the strong magnetic properties due to the high concentration of flakes, while sample MAG fails to express its full potential, as the most substantial magnetite particles are not situated in proximity to the coating's surface. Therefore, this outcome underscores a crucial consideration that is frequently overlooked: besides selecting the appropriate filler, equal importance should be placed on the ultimate structure of the coating, which plays a vital role in defining its functionality. In cases like this, with the same concentration, one additive may perform better or worse

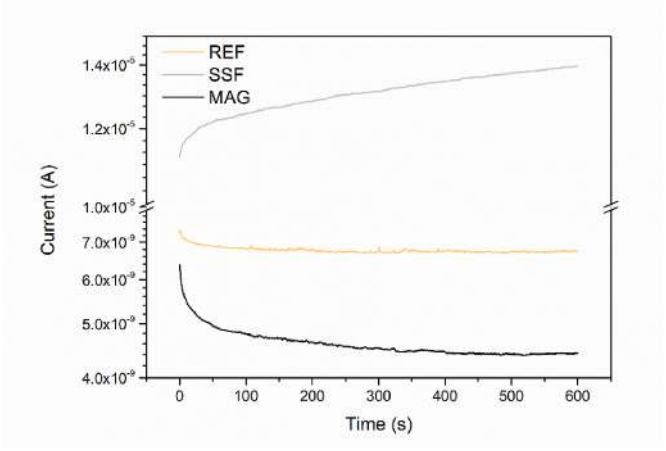

Fig. 15. Evolution of the current measured during the conductivity test.

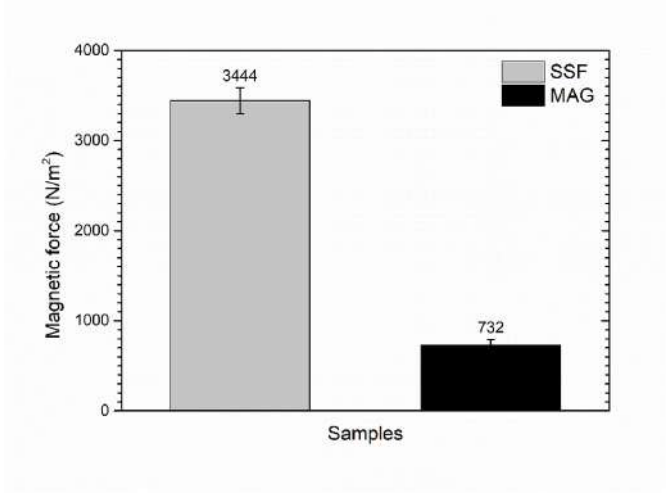

Fig. 16. Average magnetic force exploited by the two composite coatings.

than another, depending on how it is dispersed within the polymer matrix of the coating.

In summary, stainless steel flakes have shown a higher level of multifunctionality compared to magnetite powder, as evidenced by their superior electrical conductivity and strong magnetic attraction within the coating. These aspects are not solely attributed to the nature of the filler but also to the specific distribution of the additive within the polymer matrix. Both fillers have also made a significant contribution to enhancing the coating's resistance to abrasion, leveraging their distinct behavior associated with their morphology and physical-mechanical characteristics. Considering all these factors, both stainless steel flakes and magnetite powder, with a particular emphasis on stainless steel flakes, can be regarded as potential benchmarks in the development of organic composite coatings for multifunctional applications in the electronics sector, where durability and good conductivity are essential requirements.

4. Conclusions

This study delves into the effects of two distinct additives - stainless steel flakes and magnetite powder - on an acrylic bio-based wood paint, exploring their impact on visual aesthetics and multifunctionality. The analysis reveals significant coloration changes induced by these additives, leading to the paint assuming either a distinctive metallic gray or deep black hue. While these functional pigments alter the coating's structural morphology, they don't introduce notable flaws in the acrylic matrix. Consequently, incorporating both fillers can profoundly alter the coating's appearance, transforming its color and reflective attributes, introducing novel decorative elements to wood paints.

Regarding accelerated degradation experiments, both steel flakes and magnetite powders demonstrate effective UV radiation protection, preserving the sample's visual appeal to some extent. Notably, the acrylic paint's protective attributes remain unaffected by these additives, showcasing their stability against thermal stresses. Hence, these additives hold promise for outdoor coatings in environments with significant temperature fluctuations.

Liquid resistance tests highlight the stainless steel flakes' intriguing barrier properties, reducing aggressive solution absorption in the coating, thus enhancing its durability and aesthetic retention. These results endorse the use of such fillers, particularly flakes over magnetite, as functional and protective pigments for outdoor wood coatings.

Both stainless steel flakes and magnetite powder provide protective benefits, minimizing weight loss due to abrasion incidents. Additionally, flakes significantly improve the coating's overall hardness, extending its longevity. These additives serve beyond aesthetics, enhancing the acrylic matrix's mechanical properties while ensuring long-term durability. Moreover, stainless steel flakes exhibit superior versatility compared to magnetite powder, evident in their enhanced electrical conductivity and considerable magnetic force within the coating.

Summing up these findings, both stainless steel flakes and magnetite powder, with a specific emphasis on stainless steel flakes, emerge as promising standards in advancing composite coatings. These additives offer versatility in industries requiring exceptional durability, mechanical strength, electrical conductivity, and magnetic properties.

Funding

This research did not receive any specific grant from funding agencies in the public, commercial, or
not-for-profit sectors.

CRediT authorship contribution statement

Massimo Calovi: Conceptualization, Methodology, Validation, Investigation, Data curation, Writing – original draft. **Stefano Rossi:** Resources, Writing – review & editing, Supervision, Project administration.

Declaration of competing interest

The authors declare that they have no known competing financial interests or personal relationships that could have appeared to influence the work reported in this paper.

Acknowledgments

The authors greatly acknowledge the contributions of Stefano Di Blase (ICA Group, Civitanova Marche, MC, Italy), Mauro Giuriato (Eckart Italia, Rivazzano, MI, Italy) and Roberto Dante (2Dto3D, Torino, Italy) regarding the paint, the stainless steel flakes and the magnetite supply, respectively. The publication was created with the co-financing of the European Union – FSE-REACT-EU, PON Research and Innovation 2014–2020 DM1062/2021.

References

[1] Willemen R, Verstraelen H, Meskens R, Luyckx D, Vastmans K, Lenaerts S, Potters G, De Baere K. The economics of a long term coating. International Journal of Maritime Engineering 2017;159.
[2] Davis J. The effects and economic impact of corrosion. In: Corrosion: Understanding the basics. The Netherlands: ASM International Almere; 2000. p. 62–6.
[3] Khanna AS. High-performance organic coatings. Elsevier; 2008.
[4] Makhlouf ASH. Handbook of smart coatings for materials protection. Elsevier; 2014.
[5] Wu L, Guo X, Zhang J. Abrasive resistant coatings—a review. Lubricants 2014;2:66–89.
[6] Yuxuan Z, Yunyun Z, Jianrong Y, Xiaoqiang Z. Energy saving performance of thermochromic coatings with different colors for buildings. Energy Build 2020;215:109920.
[7] Wu LY, Zhao Q, Huang H, Lim R. Sol-gel based photochromic coating for solar responsive smart window. Surf Coating Technol 2017;320:601–7.
[8] Wei T, Qu Y, Zou Y, Zhang Y, Yu Q. Exploration of smart antibacterial coatings for practical applications. Current Opinion in Chemical Engineering 2021;34:100727.
[9] Baldelli A, Ou J, Barona D, Li W, Amirfazli A. Sprayable, superhydrophobic, electrically, and thermally conductive coating. Adv Mater Interfac 2021;8:1902110.
[10] Naghdi S, Rhee KY, Hui D, Park SJ. A review of conductive metal nanomaterials as conductive, transparent, and flexible coatings, thin films, and conductive fillers: different deposition methods and applications. Coatings 2018;8:278.
[11] Montemor MF. Functional and smart coatings for corrosion protection: a review of recent advances. Surf Coating Technol 2014;258:17–37.
[12] Rossi S, Russo F, Calovi M. Durability of vitreous enamel coatings and their resistance to abrasion, chemicals, and corrosion: a review. J Coating Technol Res 2021;18:39–52.
[13] Ulaeto SB, Rajan R, Pancrecious JK, Rajan T, Pai B. Developments in smart anticorrosive coatings with multifunctional characteristics. Prog Org Coating 2017;111:294–314.
[14] Radkau J. Wood: a history. Cambridge: Polity Press; 2012.
[15] Kim JK, Pal K. Recent advances in the processing of wood-plastic composites. Berlin Heidelberg: Springer-Verlag; 2010.
[16] Hoadley RB. Chemical and physical properties of wood, the structural conservation of panel Paintings: Proceedings. Part 1. Wood Science and Technology; 1998. p. 2–20.
[17] Hao J, Wu X, Oporto G, Liu W, Wang J. Structural analysis and strength-to-weight optimization of wood-based sandwich composite with honeycomb core under three-point flexural test. European Journal of Wood and Wood Products 2020;78:1195–207.
[18] Pánek M, Reinprecht L. Colour stability and surface defects of naturally aged wood treated with transparent paints for exterior constructions. Wood Res 2014;59:421–30.
[19] Zareanshahraki F, Mannari V. Formulation and optimization of radiation-curable nonisocyanate polyurethane wood coatings by mixture experimental design. J Coating Technol Res 2021;18:695–715.
[20] Bansal R, Nair S, Pandey KK. UV resistant wood coating based on zinc oxide and cerium oxide dispersed linseed oil nano-emulsion. Mater Today Commun 2022;30:103177.
[21] Jirouš-Rajković V, Miklečić J. Enhancing weathering resistance of wood—a review. Polymers 2021;13:1980.
[22] Veigel S, Grüll G, Pinkl S, Obersriebnig M, Müller U, Gindl-Altmutter W. Improving the mechanical resistance of waterborne wood coatings by adding cellulose nanofibres. React Funct Polym 2014;85:214–20.
[23] Hochmańska-Kaniewska P, Janiszewska D, Oleszek T. Enhancement of the properties of acrylic wood coatings with the use of biopolymers. Prog Org Coating 2022;162:106522.

[24] Šimůnková K, Hýsek Š, Reinprecht L, Šobotník J, Lišková T, Pánek M. Lavender oil as eco-friendly alternative to protect wood against termites without negative effect on wood properties. Sci Rep 2022;12:1–10.
[25] Miri Tari SM, Tarmian A, Azadfallah M. Improving fungal decay resistance of solvent and waterborne polyurethane-coated wood by free and microencapsulated thyme essential oil. J Coating Technol Res 2022.
[26] Nikolic M, Lawther JM, Sanadi AR. Use of nanofillers in wood coatings: a scientific review. J Coating Technol Res 2015;12:445–61.
[27] Pacheco CM, Cecilia BA, Reyes G, Oviedo C, Fernández-Pérez A, Elso M, Rojas OJ. Nanocomposite additive of SiO_2/TiO_2/nanocellulose on waterborne coating formulations for mechanical and aesthetic properties stability on wood. Mater Today Commun 2021;29.
[28] Salla J, Pandey K, Srinivasa K. Improvement of UV resistance of wood surfaces by using ZnO nanoparticles. Polym Degrad Stabil 2012;97:592–6.
[29] Janesch J, Czabany I, Hansmann C, Mautner A, Rosenau T, Gindl-Altmutter W. Transparent layer-by-layer coatings based on biopolymers and CeO2 to protect wood from UV light. Prog Org Coating 2020;138.
[30] Cheumani Yona AM, Žigon J, Ngueteu Kamlo A, Pavlič M, Dahle S, Petrič M. Preparation, surface characterization, and water resistance of silicate and Sol-Silicate inorganic–organic hybrid dispersion coatings for wood. Materials 2021;14:3559.
[31] Yang J, Li H, Yi Z, Liao M, Qin Z. Stable superhydrophobic wood surface constracting by KH580 and nano-Al2O3 on polydopamine coating with two process methods. Colloids Surf A Physicochem Eng Asp 2022:128219.
[32] Pique TM, Perez CJ, Alvarez VA, Vazquez A. Water soluble nanocomposite films based on poly (vinyl alcohol) and chemically modified montmorillonites. J Compos Mater 2014;48:545–53.
[33] Zou H, Wu S, Shen J. Polymer/silica nanocomposites: Preparation, characterization, properties, and applications. Chem Rev 2008;108:3893–957.
[34] Duan X, Liu S, Huang E, Shen X, Wang Z, Li S, Jin C. Superhydrophobic and antibacterial wood enabled by polydopamine-assisted decoration of copper nanoparticles. Colloids Surf A Physicochem Eng Asp 2020;602:125145.
[35] Cheng L, Ren S, Lu X. Application of eco-friendlywaterborne polyurethane composite coating incorporated with nano cellulose crystalline and silver nano particles on wood antibacterial board. Polymers 2020:12.
[36] Calovi M, Coroneo V, Palanti S, Rossi S. Colloidal silver as innovative multifunctional pigment: the effect of Ag concentration on the durability and biocidal activity of wood paints. Prog Org Coating 2023;175:107354.
[37] Wiemann MC. Characteristics and availability of commercially important woods. In: Forest Products Laboratory. Wood handbook: wood as an engineering material. Madison: United States Department of Agriculture: Forest Service; 2010.
[38] Yan X, Chang Y, Qian X. Effect of the concentration of pigment slurry on the film performances of waterborne wood coatings. Coatings 2019;9:635.
[39] Liu Y, Yu Z, Zhang Y, Wang H. Microbial dyeing for inoculation and pigment used in wood processing: Opportunities and challenges. Dyes Pigments 2021;186:109021.
[40] Vega Gutierrez SM, Stone DW, He R, Vega Gutierrez PT, Walsh ZM, Robinson SC. Potential Use of the pigments from Scytalidium cuboideum and Chlorociboria aeruginosa to prevent 'Greying'Decking and other outdoor wood products. Coatings 2021;11:511.
[41] Seretis G, Manolakos D, Provatidis C. On the stainless steel flakes reinforcement of polymer matrix particulate composites. Compos B Eng 2019;162:80–8.
[42] Li S, Yang J, Zhao H, Cai X, Yang B, Lu Y. The role of stainless steel flakes epoxy Intermediate nano-coating in the Heavy-duty nano organic coating system. In: IOP Conference series: materials science and engineering. IOP Publishing; 2018, 022072.
[43] Qi C, Dam-Johansen K, Weinell CE, Bi H, Wu H. Enhanced anticorrosion performance of zinc rich epoxy coatings modified with stainless steel flakes. Prog Org Coating 2022;163:106616.
[44] Russo F, Fontanari V, Rossi S. Abrasion behavior and functional properties of composite vitreous enamel coatings fabricated with the addition of 316L stainless steel flakes. Ceram Int 2022;48:23666–77.
[45] Russo F, Fontanari V, Rustighi E, Lekka M, Hernandez L, Rossi S. Composite vitreous enamel coatings with the addition of 316L stainless steel flakes: novel insights on their behaviour under mechanical stresses. Surf Coating Technol 2023;459:129393.
[46] Faulkner EB, Schwartz RJ. High performance pigments. Hoboken, USA: John Wiley & Sons; 2009.
[47] Maile FJ, Pfaff G, Reynders P. Effect pigments—past, present and future. Progress in organic coatings 2005;54:150–63.
[48] Pfaff G, Bartelt MR, Maile FJ. Metal effect pigments. Physical Sciences Reviews 2021;6:179–97.
[49] Montoya P, Martins CR, de Melo HG, Aoki IV, Jaramillo F, Calderón JA. Synthesis of polypyrrole-magnetite/silane coatings on steel and assessment of anticorrosive properties. Electrochim Acta 2014;124:100–8.
[50] Atta AM, Hameed RSA, Al-Lohedan HA, Ezzat AO, Hashem AI. Magnetite doped cuprous oxide nanoparticles as modifier for epoxy organic coating. Prog Org Coating 2017;112:295–303.
[51] Atta AM, El-Saeed AM, El-Mahdy GM, Al-Lohedan HA. Application of magnetite nano-hybrid epoxy as protective marine coatings for steel. RSC advances 2015;5:101923–31.
[52] McKeen LW. Fluorinated coatings and finishes handbook: the definitive user's guide. William Andrew; 2015.
[53] Buchheit RG. Corrosion resistant coatings and paints. In: Handbook of environmental degradation of materials. Elsevier; 2005. p. 367–85.
[54] ASTM D523-14 - Standard Test Method for Specular Gloss. West Conshohocken (PA). ASTM International; 2014. p. 1–12.
[55] ASTM G155-05. Operating Xenon Arc Light Apparatus for exposure of Non-metallic materials. West Conshohocken (PA): ASTM International; 2005. p. 1–11.
[56] UNI 9429-22. Finiture del legno e dei mobili - Determinazione della resistenza delle superfici agli sbalzi di temperatura. UNI - Ente Nazionale Italiano di Unificazione; 2022. p. 1–11.
[57] ASTM D3359-17. Standard test methods for rating adhesion by Tape test, west Conshohocken (PA). ASTM International; 2017. p. 1–10.
[58] GB/T1733-93. Determination of resistance to water of films. Beijing: Standardization Administration of the People's Republic of China; 1993. p. 1–11.
[59] EN927-05. Paints and varnishes - coating materials and coating systems for exterior wood - Part 5: assessment of the liquid water permeability. European Standard; 2005. p. 1–18.
[60] ISO 2815-2000. Determinazione della durezza con il metodo di penetrazione Buchholz. UNI - Ente Nazionale Italiano di Unificazione; 2000. p. 1–10.
[61] ASTM D4060. Standard test method for abrasion resistance of organic coatings by the Taber abraser. West Conshohocken (PA): ASTM International; 2010. p. 1–13.
[62] ASTM D257-07. Standard test methods for DC resistance or conductance of insulating materials. West Conshohocken (PA): ASTM International; 2007. p. 1–12.
[63] Calovi M, Rossi S, Deflorian F, Dirè S, Ceccato R. Effect of functionalized graphene oxide concentration on the corrosion resistance properties provided by cataphoretic acrylic coatings. Mater Chem Phys 2019;239:121984.
[64] Calovi M, Rossi S, Deflorian F, Dirè S, Ceccato R. Graphene-based reinforcing filler for double-layer acrylic coatings. Materials 2020;13:4499.
[65] Calovi M, Rossi S. The impact of stainless steel flakes as a novel multifunctional pigment for wood coatings. J Coating Technol Res 2023. Accepted.
[66] ASTM-E308-18. Standard Practice for computing the colors of objectives by using the CIE system. West Conshohocken (PA): ASTM International; 2018. p. 1–45.
[67] Mokrzycki W, Tatol M. Colour differenceΔ E-A survey. Mach Graph Vis 2011;20:383–411.
[68] Calovi M, Russo F, Rossi S. Esthetic performance of thermochromic pigments in cataphoretic and sprayed coatings for outdoor applications. J Appl Polym Sci 2021;138:50622.
[69] Calovi M, Rossi S. From wood waste to wood protection: new application of black bio renewable water-based dispersions as pigment for bio-based wood paint. Prog Org Coating 2023;180:107577.
[70] Calovi M, Rossi S. Impact of high concentrations of cellulose fibers on the morphology, durability and protective properties of wood paint. Coatings 2023;13:721.
[71] Calovi M, Rossi S. Synergistic contribution of bio-based additives in wood paint: the combined effect of pigment deriving from spirulina and multifunctional filler based on carnauba wax. Prog Org Coating 2023;182:107713.
[72] Calovi M, Rossi S. Comparative analysis of the advantages and disadvantages of utilizing spirulina-derived pigment as a bio-based colorant for wood impregnator. Coatings 2023;13:1154.
[73] Chiantore O, Trossarelli L, Lazzari M. Photooxidative degradation of acrylic and methacrylic polymers. Polymer 2000;41:1657–68.
[74] Kaczmarek H, Kamińska A, van Herk A. Photooxidative degradation of poly(alkyl methacrylate)s. Eur Polym J 2000;36:767–77.
[75] Luo H, Li X, Dong C, Xiao K, Cheng X. Influence of uv light on passive behavior of the 304 stainless steel in acid solution. J Phys Chem Solid 2013;74:691–7.
[76] Heidarinejad G, Bozorgmehr N, Safarzadeh M. Effect of highly reflective material on the performance of water ultraviolet disinfection reactor. Journal of Water Process Engineering 2020;36:101375.
[77] Sedighi A, Montazer M, Mazinani S. Fabrication of electrically conductive superparamagnetic fabric with microwave attenuation, antibacterial properties and UV protection using PEDOT/magnetite nanoparticles. Mater Des 2018;160:34–47.
[78] Yan X, Wang L, Qian X. Influence of thermochromic pigment powder on properties of waterborne primer film for Chinese fir. Coatings 2019;9:742.
[79] Yan X, Qian X, Chang Y, Lu R, Miyakoshi T. The effect of glass fiber powder on the properties of waterborne coatings with thermochromic ink on a Chinese Fir surface. Polymers 2019;11:1733.
[80] GB/T11186.3-90. Method of measurement of coating color. Part III: Calculation of chromatic Aberration. Beijing: Standardization Administration of the People's Republic of China; 1990. p. 1–12.
[81] Calovi M, Coroneo V, Rossi S. Antibacterial efficiency over time and barrier properties of wood coatings with colloidal silver. Appl Microbiol Biotechnol 2023;107:5975–86.
[82] Seretis GV, Polyzou AK, Manolakos DE, Provatidis CG. Effect of stainless steel flakes content on mechanical properties and Microstructure of Cast 96.66% pure aluminum. In: Nano Hybrids and composites. Trans Tech Publ; 2018. p. 11–9.
[83] Weidenfeller B, Höfer M, Schilling F. Thermal and electrical properties of magnetite filled polymers. Compos Appl Sci Manuf 2002;33:1041–53.
[84] Notingher P, Panaitescu D, Paven H, Chipara M. Some characteristics of conductive polymer composites containing stainless steel fibers. J Optoelectron Adv Mater 2004;6:1081–2.
[85] Elnaggar H, Graas S, Lafuerza S, Detlefs B, Tabiś W, Gala MA, Ismail A, van der Eerden A, Sikora M, Honig JM. Temperature-driven self-doping in magnetite. Phys Rev Lett 2021;127:186402.
[86] Rahman MR, Bake A, Islam SMKN, Wu L, Khakbaz H, FitzGerald S, Chalifour A, Livesey KL, Knott JC, Innis PC. Interplay between thermal and magnetic properties of polymer nanocomposites with superparamagnetic Fe3O4 nanoparticles. J Magn Magn Mater 2023;579:170859.

[87] Blachowicz T, Grzybowski J, Ehrmann A. Influence of agglomerations on magnetic properties of polymer matrices filled with magnetic nanoparticles. Mater Today Proc 2022;67:792–6.
[88] Khatri B, Lappe K, Noetzel D, Pursche K, Hanemann T. A 3D-printable polymer-metal soft-magnetic functional composite—development and characterization. Materials 2018;11:189.
[89] Palmero EM, Casaleiz D, de Vicente J, Hernández-Vicen J, López-Vidal S, Ramiro E, Bollero A. Composites based on metallic particles and tuned filling factor for 3D-printing by Fused Deposition Modeling. Compos Appl Sci Manuf 2019;124:105497.